




Cite this: *Chem. Commun.*, 2019, 55, 14996

Received 26th September 2019,
Accepted 18th November 2019

DOI: 10.1039/c9cc07517h

rsc.li/chemcomm

Hierarchy of interfacial passivation in inverted perovskite solar cells†

Tun Wang,  Sadeq Abbasi, Xin Wang, Yangrunqian Wang, Zhendong Cheng, Jiayuan Wang, Hong Liu* and Wenzhong Shen*

The crucial hierarchy of the interfacial passivation at different positions of perovskite solar cells together with the corresponding mechanism has been studied despite the selection of passivation mediums in this work. The passivation on the upper interface could more effectively enhance the device performance with an efficiency of 19.55% compared to the pristine and lower passivated cells (15.90% and 18.39%, respectively). Furthermore, the upper passivated devices exhibit better long-term and thermal stability than the lower passivated and pristine ones.

Since the first report of perovskite solar cells (PSCs) by Miyasaka *et al.*,¹ numerous works have been focused on layer modification and interfacial engineering.^{2,3} To date, the power conversion efficiency (PCE) for PSCs has been amazingly promoted to over 25%,⁴ almost comparable to silicon solar cells. In particular, the inverted (p-i-n) PSCs have shown significant advantages in terms of high stability and negligible hysteresis.⁵ Nevertheless, challenges still remain in front of their real commercialization. For instance, most deposition methods produce polycrystalline perovskites, which could contain many defects at the layer interfaces and grain boundaries that can increase the recombination and reduce the efficiency.⁶ Besides, the defects also provide possible access for moisture or oxygen outside of the device and degrade the device stability.⁷

Recently, several interface passivation approaches have been proposed to reduce the defects at the surfaces of the perovskite layer. For example, Pang *et al.* and Kazunari have used PbI_2 and a polymer as the passivation layer on top of perovskite surfaces by vapor and solution methods, respectively.^{8,9} Moreover, bifacial passivation has also been carried out to suppress non-radiative losses and reduce the defect density.¹⁰ These results have shown significantly improved open-circuit voltage (V_{OC}), short-circuit

current density (J_{SC}) and PCE and lower shunt-current leakage. However, it unclear the detailed function of the passivation on different positions of the device, and whether the passivation could affect the perovskite growth. Unbalanced carrier extraction will result in carrier aggregation at the interface and induce different effects on different positions.¹¹

In this work, we mainly focus on the passivation hierarchy and find that passivation on the upper interface is generally more efficient than that on the lower interface in inverted PSCs, which applies for polystyrene (PS), polymethyl methacrylate (PMMA) and likely other passivating systems. The utilization of the upper passivation layer can more effectively passivate surface trap states, block hole transport to the ETL, balance the extraction of carriers, and thus significantly lead to higher V_{OC} and fill factor (FF). Besides, the upper passivation layer exhibits better thermal and long-term stability for the perovskite device than that of the lower passivation layer. Such difference may have been caused by the “reparation” effect of the passivators on the perovskite layer, *i.e.*, polymeric chlorobenzene solution can enlarge the perovskite grains by minimizing the total Gibbs free energy and slowing down the perovskite crystal growth,¹² reduce the pinholes through the “cross-link” effect between the grains and suppress the ionic defects by coordination with donation of lone pair electrons.^{13,14} It also implies that the upper passivation has actually not only been “interfacial” but also a “bulk” effect. This work has clearly indicated different effects exerted on different positions of the device by the same passivation process.

Fig. 1a–c show the morphology of the prepared perovskite films *via* scanning electron microscopy (SEM) and the corresponding grain sizes have been described using histogram statistics in Fig. 1d. The pristine perovskite film was uniformly formed on the mesoporous NiO_x layer and well crystallized with very small grain size. For the lower passivated perovskite film (Fig. 1b), the grain size has been remarkably increased, which is highly attributed to the reduced wettability of the NiO_x/PS surface.¹⁵ The perovskite film with upper passivation layer also shows large grain size and its surface is much smoother than

Key Laboratory of Artificial Structures and Quantum Control (Ministry of Education), Institute of Solar Energy, School of Physics and Astronomy, Shanghai Jiao Tong University, Shanghai 200240, P. R. China. E-mail: liuhong@sjtu.edu.cn, wzshen@sjtu.edu.cn

† Electronic supplementary information (ESI) available: Materials, experimental section, additional figures and tables. See DOI: 10.1039/c9cc07517h

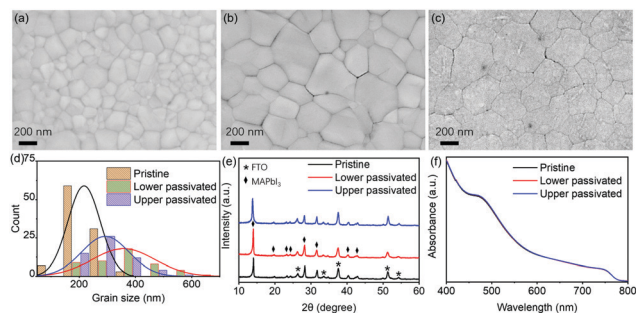


Fig. 1 Top view SEM images of (a) the pristine, (b) lower passivated and (c) upper passivated perovskite films. (d) Statistic diagram of perovskite grain size. (e) XRD patterns and (f) optical absorbance of the perovskite films without and with different passivation layers.

that of the pristine and the lower passivated ones (Fig. 1c and Fig. S2, ESI[†]). This would be beneficial for spin-coating of PCBM in the subsequent step and thereby enable better contact with the ETL on the perovskite photoactive layer. Moreover, XRD peaks of perovskite films with lower or upper passivation layers are highly similar in shape to that of the pristine film (Fig. 1e). Notably, the peak at 14.1° (corresponds to the (110) lattice reflection of MAPbI_3 structure) is significantly strengthened in the passivated samples, indicating better crystallinity. UV-vis absorption spectra of the films indicate that the absorption curves of pristine, and lower and upper passivated perovskite films are almost coincident with each other (Fig. 1f), indicating that the introduction of a passivation layer on the surface of the perovskite absorber layer will not deteriorate the perovskite itself.¹⁶

Finally, pristine planar PSCs have been fabricated with $\text{FTO}/\text{NiO}_x/\text{CH}_3\text{NH}_3\text{PbI}_3/\text{PCBM}/\text{Ag}$ architecture. Similarly, devices with $\text{FTO}/\text{NiO}_x/\text{PS}/\text{CH}_3\text{NH}_3\text{PbI}_3/\text{PCBM}/\text{Ag}$ ("lower passivated PSCs") and $\text{FTO}/\text{NiO}_x/\text{CH}_3\text{NH}_3\text{PbI}_3/\text{PS}/\text{PCBM}/\text{Ag}$ architectures ("upper passivated PSCs") were also fabricated and measured. As shown in Fig. 2a, voids and pinholes exist at the perovskite/ NiO_x interface, which could significantly weaken the contact between the perovskite and hole transport layer (HTL). Moreover,

the smaller the grain size, the more grain boundaries the photo-induced carriers will pass through, and therefore higher carrier recombination may take place, which could consequently degrade the photovoltaic performance of devices.¹⁷ Compared to that, the lower and upper passivated devices show better coverage of the perovskite layer on the substrate, with less pinholes and voids (Fig. 2b and c). In particular, the perovskite film with upper passivation layer is so compact that there are almost no visible pinholes. This could have been attributed to the cross-link effect and the ion coordination effect of the passivator precursor on the perovskite formation during the upper passivation process.¹⁴ The polymeric (such as PS and PMMA) CB solution was applied to promote the perovskite growth and film-forming properties by its cross-link effect through hydrogen bonding.¹⁸ The ultrathin insulating polymer layer can selectively conduct carriers by tunnelling effect from the perovskite layer to the HTL/ETL due to the energy-matching level for each layer,¹⁹ as illustrated in the energy diagrams in Fig. S3a and b (ESI[†]). Furthermore, lone pair electrons donated from the oxygen atoms of the polymeric Lewis bases can coordinate with perovskite crystal defects such as Pb^{2+} or NH_3^+ at grain boundaries.²⁰ All these have suggested that the upper passivation may not only affect the upper interface in the PSC, but also in the perovskite bulk itself. Hence, it is deemed to be beneficial for charge extraction and transport and thus improving the photovoltaic performance of the PSCs.

Fig. 2d shows the photocurrent density–voltage (J – V) curves of PSCs without a passivation layer and with lower PS layer and upper PS layer. The pristine device shows efficiency up to 16.39% and 16.12% under reverse and forward scanning, respectively. In comparison, the lower passivated PSC shows much better photovoltaic performances. The champion device (PS concentration 0.5 mg mL^{-1}) shows PCE up to 18.39% and 18.22% under reverse and forward scanning, respectively (detailed photovoltaic parameters of the lower and upper passivated PSCs *versus* PS concentration can be found in Fig. S3c, d and Tables S1, S2, ESI[†]). Moreover, upper passivation induced even better performance. The champion device shows PCE up to 19.55% and 19.52% at reverse and forward scanning, respectively. The J – V curves of the upper passivated device at different scanning directions are almost coincident with each other, indicating the lowest hysteresis compared to the pristine and lower passivated solar cells (detailed parameters are listed in Table S3, ESI[†]). Fig. 2e presents the external quantum efficiency (EQE) spectra of champion devices without and with a lower and upper passivation layer, respectively. The calculated J_{SC} values are well matching with the measured results shown in Table S3 (ESI[†]). Beside the champion devices, we have also made statistical analysis of the devices (Fig. S4, ESI[†]). In addition, we can obtain the values of shunt resistance (R_{sh}) and series resistance (R_{s}) from the J – V measurement. The upper passivated cell exhibits similar R_{s} with those of the lower passivated and pristine devices but much larger R_{sh} (Fig. S4a–c, ESI[†]). Generally, the higher $R_{\text{sh}}/R_{\text{s}}$ value results in higher FF,²¹ and this is consistent with our results. A considerable improvement in PCE can be expected by combining the effect of lower and upper passivation, *i.e.* bilateral passivation, which has been already verified

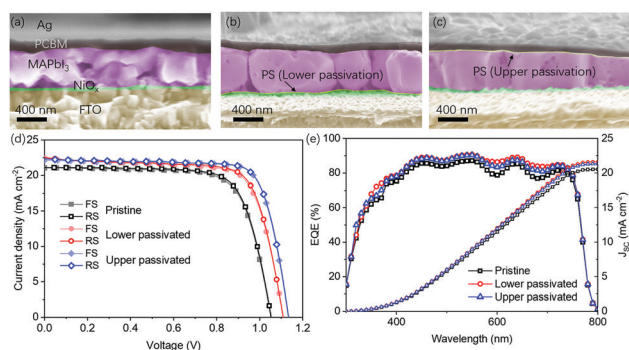


Fig. 2 False color cross-sectional SEM images of (a) the pristine perovskite solar cell without passivation layer and (b) lower passivated and (c) upper passivated PSC. (d) J – V curves of optimal PSC devices without and with lower and upper passivation layers, which were measured under different scan directions. The solid and hollow signs correspond to forward and reverse scanning, respectively. (e) The corresponding EQE and integrated J_{SC} spectra.

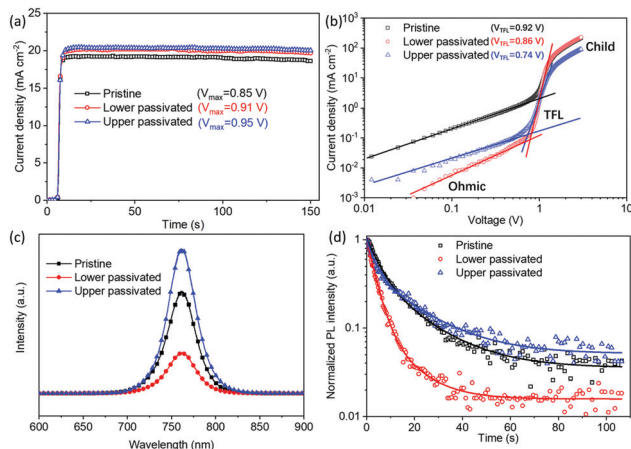


Fig. 3 (a) Steady-state output photocurrent of the champion devices. (b) Dark J - V measurement of the hole-only devices. (c) Steady-state and (d) time-resolved photoluminescence spectra of the pristine, lower and upper passivated perovskite films.

in our previous publication, and it will not be further discussed in this work.

In order to validate the reliability of the solar cell performance, we measured the steady-state current density by applying a bias voltage around the maximum output power (V_{\max}). The V_{\max} for the pristine solar cell as well as lower and upper passivated devices were calculated to be 0.85, 0.91 and 0.95 V, respectively, and the steady-state current density of the studied devices was recorded as shown in Fig. 3a. Stable PCEs of 16.28%, 18.21% and 19.24% could be achieved with photocurrents of 19.16, 20.01 and 20.25 mA cm⁻², respectively, which are consistent with the J - V measurements in Fig. 2. To evaluate the influence of passivation in such effects, the trap state density (N_{trap}) was detected by the space-charge-limited current (SCLC) method. As shown in Fig. 3b, the dark J - V curves for the hole-only devices can be divided into three distinct regions: ohmic region (left), trap-filling limited (TFL) region (middle) and child region (right).²² The N_{trap} of perovskite film can be evaluated from the trap-filling limited voltage (V_{TFL}), the onset voltage of the trap-filled limited region, using the equation $N_{\text{trap}} = 2\epsilon_0\epsilon_r V_{\text{TFL}} / (eL^2)$,⁶ where ϵ_0 is the vacuum permittivity, ϵ_r is the relative dielectric constant, e is the charge constant, and L is the thickness of the film. The values of V_{TFL} are 0.92, 0.86 and 0.74 V for the pristine, lower and upper passivated perovskite films, respectively. Therefore, the corresponding calculated trap densities are 2.65×10^{15} , 2.48×10^{15} and 2.13×10^{15} cm⁻³, respectively. The low trap density of the upper passivated device would significantly improve the performance of the PSCs.²³ Steady-state and time-resolved photoluminescence decay measurements have also been employed to investigate the charge extractions of the prepared perovskite films. The sample without passivation shows a strong steady photoluminescence (PL) peak at ~ 761 nm (Fig. 3c). As for the lower passivated sample, the PL intensity is reduced, suggesting more effective carrier transport from the perovskite absorber to the NiO_x HTL.²⁴ However, the PL intensity for the upper passivated sample is higher than that of the pristine

sample; this result might be caused by the improved perovskite film quality because of uniformly triggered heterogeneous nucleation and filling of the voids and grain boundaries by the upper PS layer.¹² This suggests that the surface non-radiative recombination defects have been largely suppressed, thus reducing the charge trapping loss.²⁵ Time-resolved photoluminescence (TRPL) decay measurements were applied to analyze the dynamics of recombination by using a 470 nm wavelength pulsed laser as the excitation source. The TRPL curves in Fig. 3d show consistent trends with the PL spectra and demonstrate an obvious biexponential decay behavior containing a fast decay (τ_1) component followed by a slow decay process (τ_2) (details are listed in Table S4, ESI†). Compared to the pristine sample with average lifetime (τ_a) of 13.3 ns, the PL quenching of the lower passivated sample is significantly enhanced ($\tau_a = 5.8$ ns), which is mainly attributed to improved charge transfer.²⁴ The insignificant lifetime recovery after introducing the upper passivation layer indicates reduced interface recombination and efficient passivation effect.¹² The surface trap states and nonradiative recombination centers are attenuated in the perovskite layer protected by the upper PS, resulting in higher V_{OC} of the corresponding PSCs.²⁶

Furthermore, electrochemical impedance spectroscopy (EIS) measurements were implemented at a bias voltage of 0.8 V in the dark to evaluate the charge transport process and contact resistance (Fig. 4a). The arc in the high frequency region indicates that the upper passivated device shows the highest recombination resistance. Besides, the information of R_s values can be evaluated from the x -intercept in the left part of the arc (Fig. S5, ESI†), both of which are consistent with the above discussion. In addition, the capacitance-voltage (C - V) characteristics obtained from Mott-Schottky measurements were also performed to evaluate the passivation effect. The built-in potential (V_{bi}) can be extracted from the x -intercept (Fig. 4b), and the values are 0.94, 1.00 and 1.06 V for pristine, lower and upper passivated devices, respectively. The enlarged V_{bi} can not

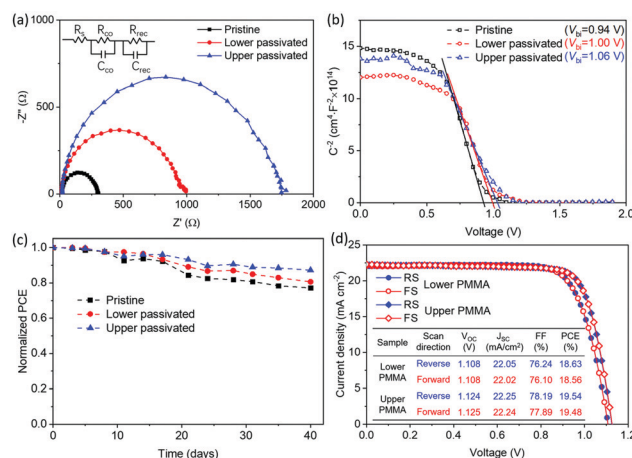


Fig. 4 (a) EIS Nyquist plots (inset: fitting circuit), (b) Mott-Schottky curves and (c) long-term stability of the pristine, lower and upper passivated PSCs. (d) J - V curves of optimal PSCs with lower and upper PMMA passivation layer (inset: detailed photovoltaic parameters). The solid and hollow signs correspond to reverse and forward scanning, respectively.

only extend the depleted region and suppress the back transport of holes from the HTL to the perovskite layer, but also accelerate charge dissociation and avoid charge accumulation at the HTL/perovskite interface and thus contribute to higher V_{OC} .²⁷ Apart from the increased photovoltaic parameters, the passivation layer affects the device stability as well. We measured long-term stability of the champion devices under the same conditions without encapsulation, stored in a drying cabinet (at $\sim 22^\circ\text{C}$ and relative humidity of $\sim 2\%$). The upper and lower passivated PSCs retained around 87% and 85% of their initial PCE values after 40 days of storage, respectively, whereas that of the pristine PSC was reduced to almost 77% of its initial value (Fig. 4c). Besides, the upper passivated perovskite film exhibits much better thermal stability than those of the pristine and lower passivated ones measured at 120°C in air with humidity of 60% (Fig. S6, ESI†). This can be explained by the fact that the upper passivated perovskite film is protected by the PS film, which can effectively inhibit perovskite decomposition by blocking water invasion.²⁸ We have also verified that bilaterally passivated samples show similar thermal stability to that of the upper passivated one in our previous work, suggesting the upper passivation film plays a dominant role in preventing the decomposition of the perovskite layer. To further verify the universality of such a hierarchy in other passivation systems, we have also introduced PMMA to the devices. The prepared perovskite films with lower and upper PMMA passivation film exhibit similar trends with those of the PS-passivated samples (Fig. S7 and S8, ESI†). Then we fabricated lower and upper passivated PSCs and measured their $J-V$ curves (Fig. 4d). The upper passivated PSC exhibits a champion PCE of 19.54%, which is higher than that of the lower passivated device (18.63%). The inset lists the detailed photovoltaic parameters, indicating that the major promotion of the upper-passivated PSCs also comes from the enhanced V_{OC} . Similar to the PS case, the passivation by PMMA also shows positive proportion of contact angle with increasing passivator concentration, which can effectively tailor the nucleation and growth process of perovskite grains.²⁹ In general, for other possible candidates of passivators such as phenethylammonium iodide and polyethylene glycol,^{25,30} this hierarchy effect could also very possibly exist. Concerning the dual effects of upper passivation on the top interface and perovskite bulk, even better performance could be induced if it could be reproduced in other positions of the device.

In summary, we have clearly demonstrated that passivation of the upper interface would be in principle more efficient than that of the lower interface in PSCs. Such a difference has been apparently attributed to the “reparation” effect of passivation medium on the perovskite layer, which has effectively filled the grain boundaries of the perovskite layer and reduced the trap state density in both the perovskite layer and the interface between it and the upper carrier transport layer. A PCE of 19.55% and V_{OC} of 1.133 V with negligible hysteresis have been achieved for the champion devices with an upper passivation layer. Comparing to the pristine and lower passivated devices, the upper passivated PSC exhibits better long-term and thermal stability. The difference has indicated that the upper passivation may not only induce “interfacial” but also “bulk” effects on the devices. Such a result

could hopefully facilitate the passivation in PSC devices in general with other modifications and different materials.

This work was supported by the Natural Science Foundation of China (11834011, 11674225, 11474201, and 11204176).

Conflicts of interest

There are no conflicts to declare.

Notes and references

- 1 A. Kojima, K. Teshima, Y. Shirai and T. Miyasaka, *J. Am. Chem. Soc.*, 2009, **131**, 6050–6051.
- 2 B. Roose, Q. Wang and A. Abate, *Adv. Energy Mater.*, 2018, **9**, 1803140.
- 3 J. Shi, X. Xu, D. Li and Q. Meng, *Small*, 2015, **11**, 2472–2486.
- 4 NREL, Efficiency chart, <https://www.nrel.gov/pv/assets/pdfs/best-research-cell-efficiencies.20190802.pdf>, (accessed August 2019).
- 5 J. Zhang, H. Luo, W. Xie, X. Lin, X. Hou, J. Zhou, S. Huang, W. Ou-Yang, Z. Sun and X. Chen, *Nanoscale*, 2018, **10**, 5617–5625.
- 6 T. Wu, Y. Wang, X. Li, Y. Wu, X. Meng, D. Cui, X. Yang and L. Han, *Adv. Energy Mater.*, 2019, **9**, 1803766.
- 7 T. Leijtens, G. E. Eperon, N. K. Noel, S. N. Habisreutinger, A. Petrozza and H. J. Snaith, *Adv. Energy Mater.*, 2015, **5**, 1500963.
- 8 Z. Li, C. Zhang, Z. Shao, Y. Fan, R. Liu, L. Wang and S. Pang, *J. Mater. Chem. A*, 2018, **6**, 9397–9401.
- 9 F. Wang, A. Shimazaki, F. Yang, K. Kanahashi, K. Matsuki, Y. Miyauchi, T. Takenobu, A. Wakamiya, Y. Murata and K. Matsuda, *J. Phys. Chem. C*, 2017, **121**, 1562–1568.
- 10 Y. Zhao, Q. Li, W. Zhou, Y. Hou, Y. Zhao, R. Fu, D. Yu, X. Liu and Q. Zhao, *Sol. RRL*, 2019, **3**, 1800296.
- 11 K. Chen, Q. Hu, T. Liu, L. Zhao, D. Luo, J. Wu, Y. Zhang, W. Zhang, F. Liu, T. P. Russell, R. Zhu and Q. Gong, *Adv. Mater.*, 2016, **28**, 10718–10724.
- 12 D. Bi, C. Yi, J. Luo, J. D. Décoppet, F. Zhang, S. M. Zakeeruddin, X. Li, A. Hagfeldt and M. Grätzel, *Nat. Energy*, 2016, **1**, 16142.
- 13 Y. Zhao, J. Wei, H. Li, Y. Yan, W. Zhou, D. Yu and Q. Zhao, *Nat. Commun.*, 2016, **7**, 10228.
- 14 T. H. Han, J. W. Lee, C. Choi, S. Tan, C. Lee, Y. Zhao, Z. Dai, N. De Marco, S. J. Lee, S. H. Bae, Y. Yuan, H. M. Lee, Y. Huang and Y. Yang, *Nat. Commun.*, 2019, **10**, 520.
- 15 C. Bi, Q. Wang, Y. Shao, Y. Yuan, Z. Xiao and J. Huang, *Nat. Commun.*, 2015, **6**, 7747.
- 16 F. Wu, X. Yue, Q. Song and L. Zhu, *Sol. RRL*, 2018, **2**, 1700147.
- 17 Z. Xiao, Q. Dong, C. Bi, Y. Shao, Y. Yuan and J. Huang, *Adv. Mater.*, 2014, **26**, 6503–6509.
- 18 Z. Lin, J. Chang, H. Zhu, Q.-H. Xu, C. Zhang, J. Ouyang and Y. Hao, *Sol. Energy Mater. Sol. Cells*, 2017, **172**, 133–139.
- 19 Q. Wang, Q. Dong, T. Li, A. Gruverman and J. Huang, *Adv. Mater.*, 2016, **28**, 6734–6739.
- 20 L. Zuo, H. Guo, D. W. Dequillettes, S. Jariwala, M. N. De, S. Dong, R. Deblock, D. S. Ginger, B. Dunn and M. Wang, *Sci. Adv.*, 2017, **3**, e1700106.
- 21 N. Mundhaas, Z. J. Yu, K. A. Bush, H. P. Wang, J. Häusele, S. Kavadiya, M. D. McGehee and Z. C. Holman, *Sol. RRL*, 2019, **3**, 1800378.
- 22 T. Niu, J. Lu, R. Munir, J. Li, D. Barrit, X. Zhang, H. Hu, Z. Yang, A. Amassian, K. Zhao and S. F. Liu, *Adv. Mater.*, 2018, **30**, 1706576.
- 23 X. Zhang, D. Yang, R. Yang, X. Zhu, J. Feng, Z. Wang, S. Zuo, J. Niu and S. Liu, *Org. Electron.*, 2018, **62**, 499–504.
- 24 Q. Wang, C. C. Chueh, T. Zhao, M. Eslamian, W. Choy and A. K. Jen, *ChemSusChem*, 2017, **10**, 3794–3803.
- 25 Q. Jiang, Y. Zhao, X. Zhang, X. Yang, Y. Chen, Z. Chu, Q. Ye, X. Li, Z. Yin and J. You, *Nat. Photonics*, 2019, **13**, 460–466.
- 26 F. Yang, H. E. Lim, F. Wang, M. Ozaki, A. Shimazaki, J. Liu, N. B. Mohamed, K. Shinokita, Y. Miyauchi, A. Wakamiya, Y. Murata and K. Matsuda, *Adv. Mater. Interfaces*, 2018, **5**, 1701256.
- 27 G. Yang, C. Wang, H. Lei, X. Zheng, P. Qin, L. Xiong, X. Zhao, Y. Yan and G. Fang, *J. Mater. Chem. A*, 2017, **5**, 1658–1666.
- 28 I. Hwang, I. Jeong, J. Lee, J. K. Min and K. Yong, *ACS Appl. Mater. Interfaces*, 2015, **7**, 17330.
- 29 Y. Du, C. Xin, W. Huang, B. Shi, Y. Ding, C. Wei, Y. Zhao, Y. Li and X. Zhang, *ACS Sustainable Chem. Eng.*, 2018, **6**, 16806–16812.
- 30 Y. Cai, Z. Zhang, Y. Zhou, H. Liu, Q. Qin, X. Lu, X. Gao, L. Shui, S. Wu and J. Liu, *Electrochim. Acta*, 2018, **261**, 445–453.